Virology 385 (2009) 39–46

Contents lists available at ScienceDirect

Virology

journal homepage: www.elsevier.com/locate/yviro

# Growth of an RNA virus in single cells reveals a broad fitness distribution

Ying Zhu, Andrew Yongky, John Yin *

*Department of Chemical and Biological Engineering, University of Wisconsin-Madison, Madison, WI 53706-1607, USA*

ARTICLE INFO

*Article history:*
Received 24 June 2008
Returned to author for revision
8 August 2008
Accepted 13 October 2008
Available online 13 December 2008

*Keywords:*
Fitness distribution
Cell cycle
Vesicular stomatitis virus
Quasi-species

ABSTRACT

Genetic and environmental factors will influence the growth of an RNA virus, but their relative contributions are challenging to resolve because standard culture methods mask how virus particles interact with individual host cells. Here, single particles of vesicular stomatitis virus, a prototype RNA virus, were used to infect individual BHK cells. Infected cells produced 50 to 8000 progeny virus particles, but these differences were lost upon subsequent culture, suggesting the diversity of yields reflected cell-to-cell differences rather than viral genetic variation. Cells infected at different phases of their cell cycle produced from 1400 (early S) to 8700 ($G_2$M) infectious virus particles, coinciding with the middle-to-upper range of the observed distribution. Fluctuations in virus and cell compositions and noisy gene expression may also contribute to the broad distribution of virus yields. These findings take a step toward quantifying how environmental variation can impact the fitness distribution of an RNA virus.



## Introduction

Although RNA viruses employ different strategies to reproduce within their host cells, they share two requirements for growth. They require their own polymerases for replication of their RNA genomes, and like all viruses, they depend on host-cellular resources for biosynthesis of their nucleic acids and proteins. A distinguishing feature of the viral RNA-dependent RNA polymerases is the highly error-prone nature of their processing (Drake and Holland, 1999; Gohara et al., 2004; and Steinhauer et al., 1992), which couples viral genome replication with genetic diversification of the virus progeny released from infected cells. Consequently, RNA viruses exist as genetically heterogeneous populations (Domingo et al., 1985; Goodenow et al., 1989; and Holland, 1993), and this genetic heterogeneity enables them to adapt to new host environments (Demma et al., 2005; and Parrish and Kawaoka, 2005), including environments containing antiviral drugs (Domingo, 2003). Moreover, mounting evidence suggests that the within-host genetic diversity of RNA virus populations plays a significant role in their pathogenicity (Aaskov et al., 2006; Carrillo et al., 2007; Farci et al., 2000; and Vignuzzi et al., 2006). Despite progress that has linked viral genetic variation to the functional diversity, adaptability and natural persistence of RNA viruses, little attention has been devoted toward understanding how factors beyond viral genetic differences, such as variation across host environments, can impact virus growth. The problem is challenging in part because potentially important cell-to-cell differences will be masked by standard culture methods that only provide average-virus or average-cell behaviors. We address this issue by measuring virus progeny yields from single cells infected by single particles of vesicular stomatitis virus (VSV), an RNA virus that exists as a quasi-species (Cuevas et al., 2005; Marcus et al., 1998; and Steinhauer et al., 1989) and ranks among the most widely investigated systems for the study of viral evolution (Duarte et al., 1993; Elena et al., 1996; Holland et al., 1982; Nichol et al., 1989; Novella et al., 1999, 2007; Quer et al., 2001; and Sanjuan et al., 2007). We infect cells with a recombinant strain of VSV that expresses green-fluorescent protein, and we employ fluorescence-activated cell sorting (FACS) to isolate individual cells that have been infected by single virus particles.

## Results and discussion

### *Infections of individual cells by single virus particles*

To detect, quantify and isolate single BHK cells infected by single virus particles we initially employed flow cytometry to test cells infected at MOI 0.01 with a recombinant strain of VSV that expresses green fluorescent protein (GFP). The low MOI was used to minimize the likelihood that any cell was infected by more than one virus particle; 99.5% of the cells should receive zero of one virus particle at MOI 0.01, assuming particles are distributed to cells as a Poisson process. A GFP signal was apparent at 3 h post infection (HPI), and the intensity increased between 3 and 5 HPI (Fig. 1a), indicative of infection-mediated expression of GFP. Infected cells could be distinguished from non-infected or dead cells at different times based on the intensities of their fluorescence signatures shown in the lower right quadrant of the panels in Fig. 1a. Dead cells, which were discarded, were detected based on their uptake of propidium iodide (PI) and the resultant signal in the PI channel. Further, the fraction of detectable infected cells and their level of GFP expression increased

* Corresponding author. Fax: +1 608 262 5434.
*E-mail address:* yin@engr.wisc.edu (J. Yin).

0042-6822/$ – see front matter © 2008 Elsevier Inc. All rights reserved.
doi:10.1016/j.virol.2008.10.031

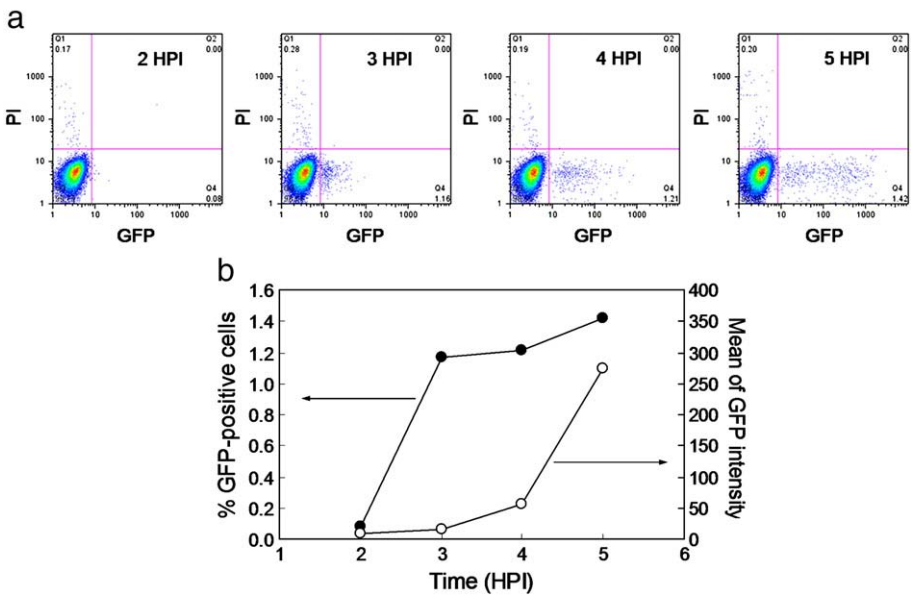


**Fig. 1.** Detection and quantification of GFP by FACS. (a) Pseudo-color plots of PI intensity and GFP intensity at 2, 3, 4 and 5 h post-infection (HPI) for BHK cells infected with VSV-GFP at MOI 0.01. Events range from high density (red) to low density (blue). Region Q4 at the lower right defines the population of live (PI-negative) and infected (GFP-positive) cells. (b) Change in percentage of GFP-positive cells and mean GFP intensity (arbitrary units) with time post-infection (hours).

monotonically between 2 and 5 HPI (Fig. 1b), consistent with the timing of protein expression in VSV infections.

*Insensitivity of virus production to sorting of infected cells*

The isolation and characterization of single infected cells required sample-processing steps that could potentially influence quantitative measurements of virus production. These steps included treatment of cells with trypsin, resuspension in fresh media, cooling on ice, and cell sorting. To test how these processes collectively impact virus production, infected cells were sorted into multiple subpopulations, each containing 500 cells, and these subpopulations were then cultured, sampled at different times, and assayed for viral progeny. The resulting one-step growth behavior for sorted cells followed a trajectory that was indistinguishable from control cells that had not been sorted (Fig. 2), indicating that sample processing had no detectable effects on the production of virus from infected cells. Together, the results from Figs. 1b and 2 indicate 3 HPI as an appropriate point for detection and sorting of infected cells, a point that preceded the start of detectable virus progeny release.

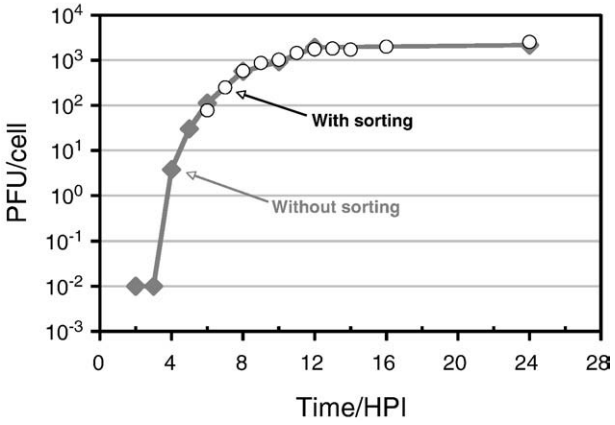


**Fig. 2.** One-step growth curves of BHK cells with and without sorting. Cells infected at MOI 5 were either sorted (open circles) or not sorted (solid diamonds) and production of viral progeny was determined.

*Virus fitness distribution*

The fitness of a virus particle may be defined as the total number of viral progeny produced when the virus infects a susceptible cell. Fitness distributions may then be measured by quantifying the yield or "burst size" from multiple individual cells, each infected by a single virus particle. Fluorescence-activated cell sorting was used to isolate 192 infected cells and the resulting distribution of virus yields from productive cells, shown in the upper panel of Fig. 3, spanned from 50 plaque-forming units per cell (PFU/cell) to 8000 PFU/cell, with a mean of 2650 PFU/cell and a relative standard deviation of approximately 15%. Although all the selected cells exhibited successful initiations of infection, based on their expression of GFP, 30% of these cells (58 out of 192) were below our detection limit for the production of virus. Infections in these cells may have gone undetected because the cells simply produced little or no virus or because trajectories of isolated cell-containing droplets missed their target wells (Tyrer and Kunkel-Berkley, 1984). Virus yields determined for the remaining 134 infected cells provided the observed distribution of virus fitness.

To assess a potential contribution of viral genetic heterogeneity on the broad fitness distribution progeny viruses descended from low- and high-yield sub-populations were further tested. If genetic variation contributed to the observed distribution in fitness, the low- and high-fitness virus phenotypes should to some extent be transferable and detectable from one generation to the next. As shown in Fig. 3 (lower panel), seven descendents of low-fitness virus, drawn from samples of the initial distribution that produced between 10 PFU/cell and 500 PFU/cell, and eight descendents of high-fitness virus, drawn from samples of the initial distribution that produced more than 4500 PFU/cell, were amplified and characterized by one-step growth cultures. None of these 15 descendents of the initial population produced similar yields as their parental populations. Five descendents of low-fitness viruses and all eight descendents of high-fitness viruses produced progeny yields that were essentially indistinguishable from each other, within 15% of 2550 PFU/cell. The remaining two descendents of the low-fitness virus produced lower-than-average yields at 1125 PFU/cell (descendent 1) and 1594 PFU/cell (descendent 2), which were significantly lower than the yields from the other 13 descendents ($P<0.0005$). The persistence of the low-fitness phenotype during culture indicates a genetic contribution to the variation in

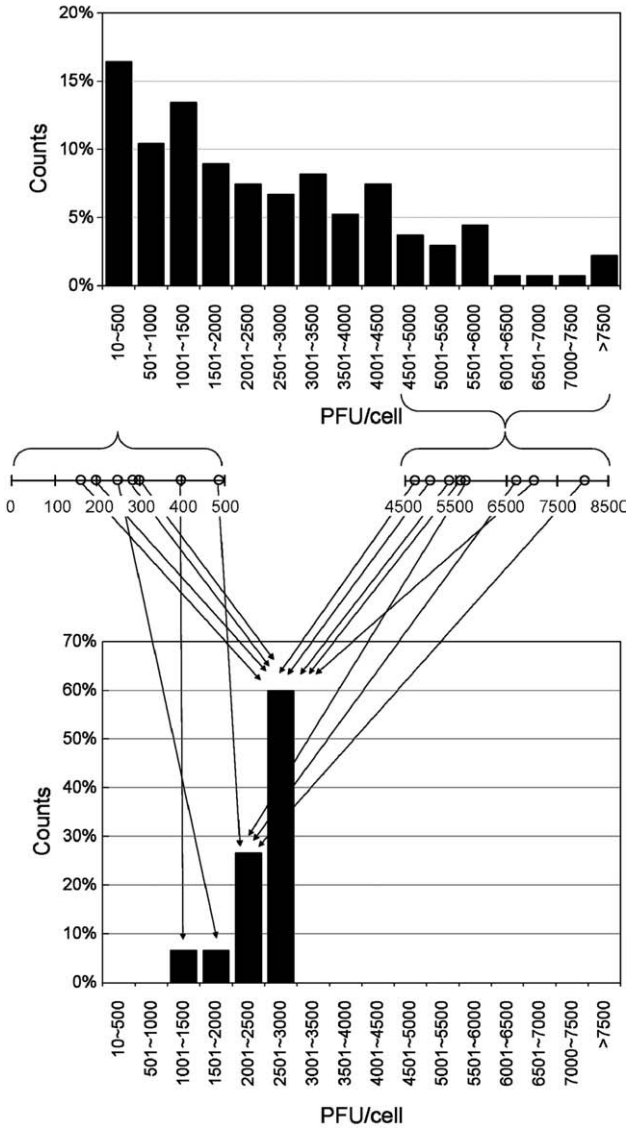


**Fig. 3.** Fitness distribution from single-cell yields of virus production. (Upper panel) Cells infected at low MOI were sorted and yields of virus progeny were determined. (Lower panel) Persistence of different growth phenotypes was tested by measuring growth yields from viruses descended from high- and low-yield infections.

fitness of these two isolates that is lacking in the other 13 isolates. The low fitness of these two isolates was further reflected by average plaque size measurements of 0.7 mm and 1.0 mm respectively, which fell below the 1.2±0.1 mm value measured from one of the average-yield descendents and the high-yield descendents (not shown).

One might attribute the apparent loss or gain of fitness by the initial high- or low-fitness viruses to genetic changes that arose during their amplification. Our amplification of the high-fitness viruses involved neither repeated genetic bottleneck (plaque-to-plaque) passaging nor changes in growth conditions that can reduce the fitness of RNA viruses (Chao, 1990), including VSV (Duarte et al., 1992; and Elena and Moya, 1999). Moreover, genetic bottleneck passaging followed by large-population passaging can give rise to gains in the fitness of VSV populations (Clarke et al., 1993; and Miralles et al., 1999), but the low-fitness viruses in this study were not cultured under such conditions. While it is unlikely, it remains conceivable that compensatory loss- or gain-of-fitness mutations in the high- and low-fitness isolates, respectively, occurred during amplification. Differences between parental and descendent virus yields might be attributed to differences in their determination; parental virus yields were measured from individual cells infected by single virus particles while descendent yields were measured from one-step virus cultures performed at MOI 5. However, when yield distributions were determined for cell cultures infected over the range of MOI in this study negligible differences were observed (Figure S1). In light of these observations, the lack of correlation between parental and descendent virus yields in Fig. 3 (upper versus lower panels) indicate that genetic differences among individual virus particles cannot account for the broad distribution of yields in Fig. 3 (upper panel).

*Virus fitness correlates with host-cell size*

To reproduce, viruses rely on the biosynthetic machinery of the cells they infect. Larger cells may provide more resources for biosynthesis than smaller cells, so the total yield of viral progeny from an infected cell may correlate with the size of the cell. FACS was implemented to divide cells into high-, medium-, and low-forward scattering (FSC) populations (Fig. 4a), and confirmed by microscopy that the measures of FSC correlated with cell size (Fig. 4b), as expected from theory (Sharpless and Melamed, 1976). These subpopulations of infected cells, which ranged in average size from 14 to 20 μm, produced average virus yields of 2200 to 2900 PFU per cell, respectively (Fig. 4c), consistent with the idea that larger cells can produce more viral progeny. If one extrapolates these measured relationships from the extreme observed values of FSC to estimate the corresponding cell size and yield, then cell sizes spanning 8 to 24 μm

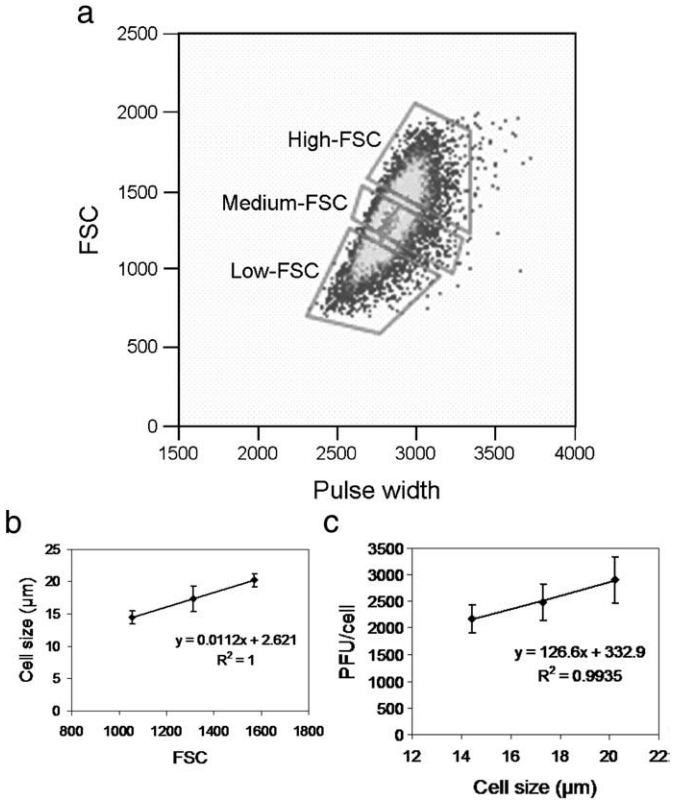


**Fig. 4.** Virus yield dependence on cell size. (a) Infected cells divided into three groups based on their FSC intensity and pulse width. High-FSC, medium-FSC and low-FSC cell populations accounted for 25%, 50% and 25% of the cells respectively, and the mean value of FSC was determined for each group. (b) Cell size relationship to FSC. One set of collected cells was imaged by an inverted epifluorescent microscope with a CCD camera. For each group, approximately 100 cells were manually measured from phase-contrast images and their sizes were averaged. A parallel set of collected cells was cultured until 24 HPI and the supernatants were titered by plaque assay. (c) Relationship of virus yield to cell size.

would produce virus yields of 1300 to 3400 PFU per cell, respectively, falling short of the observed 50-to-8000 PFU per cell range observed in Fig. 3. Alternatively, one may argue that virus yields should scale with the volume of cellular resources, so a three-fold range of cell diameters would give a 27-fold range of cell volumes, which is far short of the 160-fold range of virus yields. Similarly, Delbrück's classic study of bacteriophage yields from single infected bacterial cells showed a greater than 20-fold range of phage progeny yields while bacterial host cells only differed by 3-fold in volume (Delbrück, 1945). An alternative interpretation of our results is that cells become larger

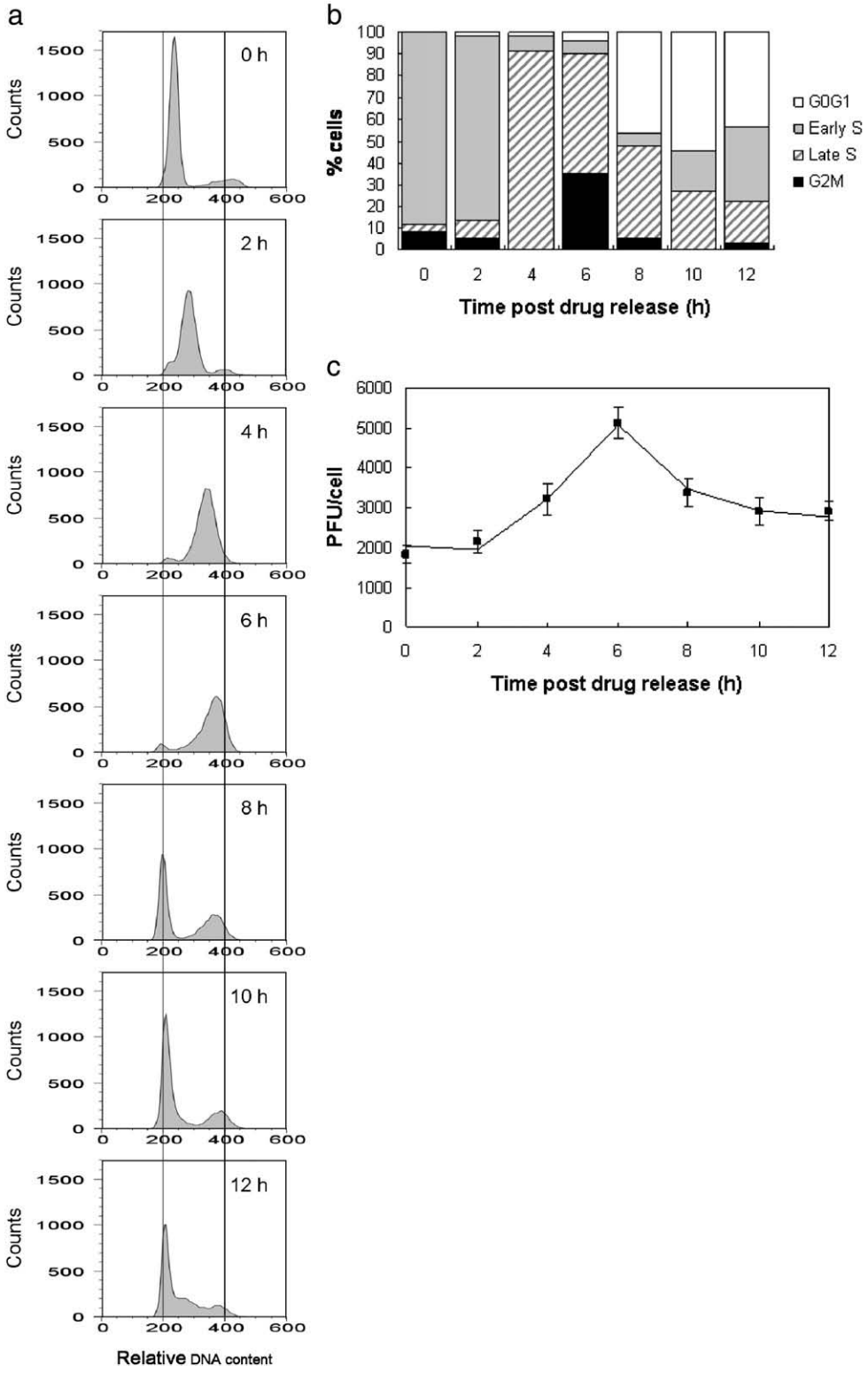


**Fig. 5.** Effects of cell cycle on virus yield. (a) Change in DNA content of cells following release from aphidicolin treatment. (b) Distribution of cells in different phases of the cell cycle as determined by ModFit. Cells are in $G_2M$ (black), late S (hatched), early S (gray), and $G_0G_1$ (white) phases. (c) Virus yields from BHK cells infected at different times following release from aphidicolin treatment. Measured virus yields (black squares) and super-position model (black line) are shown. Four replicate measurements were performed for each time point.

as a consequence of more efficient virus replication. Rounding of cells occurs at about 4 HPI owing to the expression of the VSV matrix protein (Blondel et al., 1990), and such rounding could be correlated with changes in cell size. It remains an open question whether variations in the expression of VSV matrix protein or other mechanisms might influence the cell size distribution.

*Virus fitness reflects phase of cell cycle*

As cells grow and divide they progress through a cycle of phases that include gap 1 ($G_1$), DNA synthesis (S), gap 2 ($G_2$), and cell division or mitosis (M). When a cell leaves the cycle, either temporarily or permanently, it may further become "quiescent" ($G_0$). To test the effects of cell phase on virus production, we initially arrested cells at the $G_1$/S boundary with aphidicolin (Foisy and Bibor-Hardy, 1988; and Pedrali-Noy et al., 1980), released this drug block, and tracked the progress of the resulting cell populations over 12 h. Measurements of cellular DNA levels showed a regular pattern of progression of the cells as a population through the cell cycle (Fig. 5a). Cells synthesize DNA, indicated by the increase in DNA signal from 0 to 6 h following release of the $G_1$S block, and the shift in the intensity of this signal from high to low between 6 and 8 h reflects cell division. The corresponding distribution of cells across different phases of the cell cycle, estimated from these DNA distributions, indicated that the cells initially populated primarily the early S phase, progressed to the late S phase, and then to the $G_2$M phase (Fig. 5b), as expected. Cells in two or more phases, starting at 6 h, reflect some loss of synchrony as the cells either progressed through or entered the cell cycle. When cells at these different phases were infected at MOI 5, they produced average virus yields spanning from 1800±200 PFU/cell to 5100±400 PFU/cell, as shown in Fig. 5c (data points). By contrast, the non-synchronized cell population produced an average of 2500±200 PFU/cell. A simple super-position model, which accounted well for the observed yields (Fig. 5c, lines), provided estimates for virus yields from each phase of the cell cycle, summarized in Table 1. The predicted virus yield from an infection of non-synchronous cells, based on measured distributions in cell cycle and the values in Table 1, gave a value of 2900 PFU/cell, about 12% higher than our experimental observations, providing an estimate of uncertainty associated with our model. Our observations suggest cells enriched in the $G_2$M phase, when infected, would produce a higher average yield than non-synchronized cells, and this prediction has been verified (Figure S2). Overall, segregation of cells based on their cell-cycle phase produced a broader range of virus yields than our segregation based on cell size, suggesting that the phase of the cell provides a better foundation for understanding how the resources of the host quantitatively influence the production of viral progeny.

*Fitness distributions reflect coupling of genetic, environmental and other factors*

By characterizing how different factors contribute to the distribution of virus growth phenotypes, we have initially sought simple underlying mechanisms. Here we explore the potential multi-layered nature of interactions between genomes and their environments.

**Table 1**
Parameters for the simple super-position model

| Cell stage | Paramaters (PFU/cell) | 95% confidence intervals |
|---|---|---|
| G2M | 8684 | (6675, 10693) |
| Late S | 3344 | (2682, 4006) |
| Early S | 1367 | (855, 1878) |
| G0G1 | 3246 | (2397, 4096) |

Values and 95% confidence intervals for virus yields from each phase of the cell cycle were estimated by multiple regression.

Genetic differences among clones were identified here based on the persistence of two out of seven low-yield phenotypes from one generation to the next. Owing to the high genetic variability of VSV populations (Steinhauer et al., 1989), we would expect many viruses within our initial population to be genetically different but indistinguishable from each other based on phenotypic measures of average virus yield or plaque size. By genome sequencing and further study of the two persistent low-yield strains, one might well identify relevant mutations and suggest mechanisms that account for their effects on growth phenotype. Such studies have been performed for VSV (Novella and Ebendick-Corpus, 2004; and Novella et al., 2005) and many other viruses (Carrillo et al., 2007; Duffy et al., 2006; Larder and Kemp, 1989; Poon and Chao, 2006; and Yen et al., 2005). We found the $G_2$M transition to be a highly productive environment for VSV growth in BHK cells and suggested that viruses use the resources that they encounter by chance in a susceptible cell. However, one should note that viruses can also actively influence their host-cell environments. Many viruses, including papillomaviruses, Epstein–Barr virus and human T-cell leukemia virus type I, encode genes that actively alter the cell cycle by deregulating cell growth and division, processes that can promote cancer (Butel, 2000). Moreover, RNA viruses, DNA viruses and retroviruses have evolved diverse mechanisms to specifically arrest the cell cycle at the $G_2$M transition (Davy and Doorbar, 2007), and studies of a positive-strand RNA coronavirus indicate that viral-mediated arrest at the $G_2$M transition provides favorable conditions for viral replication (Dove et al., 2006). It is not yet known how the $G_2$M transition, beyond contributions from biosynthetic resources that scale with cell size, enhances VSV growth or whether VSV possesses mechanisms to actively arrest cells at $G_2$M.

In addition to genetic and cell size or cell-cycle effects, fluctuations in virus particle and cell compositions, as well as stochastic gene expression, may well contribute to cell-to-cell differences in virus yield. A single VSV particle releases one negative-strand RNA genome and about 50 RNA-dependent RNA polymerase molecules into its host cell (Thomas et al., 1985). Differences in the levels of packaged and released polymerase during the earliest stages of infection, could be amplified owing to fluctuations in levels of cellular resources, including precursors essential for RNA and protein synthesis. Even in the absence of differences in virus or host resource levels stochastic fluctuations associated with small numbers of reactive species may also plausibly contribute to a broad distribution of virus progeny yields. For example, computer simulations (Arkin et al., 1998; Srivastava et al., 2002; and Weinberger et al., 2005) and experiments (Weinberger et al., 2005) of gene regulatory components of lambda phage, HIV and hepatitis B virus have exhibited 10- to 100-fold differences in gene expression owing to amplification of intrinsic fluctuations in reaction rates.

The persistence of viruses in nature depends on their ability to grow and spread, encompassing processes that span from encounters with single cells to spread among multi-cellular host organisms. Owing to these different lengths and time scales over which virus infections act, different measures of fitness may be appropriate. Here we have defined the fitness of an individual virus particle by the yield of offspring virus particles that are produced when it infects a single host cell. If host cells are available in excess of virus particles, competition among different virus strains for cells, perhaps over multiple generations of virus growth, may define alternative measures of fitness based, for example, on the rate rather than yield of virus production (Cuevas et al., 2005). In the presence of anti-viral drugs, fitness may be defined by whether or not virus strains carry mutations for drug-resistance. Moreover, fitness may be defined by an ability of a virus strain to escape surveillance and destruction by the innate or adaptive immune defenses of the infected host (Pfeiffer and Kirkegaard, 2006). Advances in our ability to reliably and precisely quantify other measures of fitness will motivate a need to better understand how they are quantitatively influenced by genetic, environmental, and stochastic factors.

## Materials and methods

### *Cell culture*

Baby hamster kidney (BHK-21) cells originally obtained from Isabel Novella (Medical College of Ohio) were grown as monolayers at 37 °C in a humidified atmosphere containing 5% $CO_2$. Growth medium consisted of Minimum Essential Medium Eagle with Earle's Salts (MEM, Cellgro), 10% fetal bovine serum (FBS, Hyclone), and 2 mM Glutamax I (Glu, Gibco). Cells were subcultured approximately every fourth day. For subculture, monolayers were rinsed with Hank's Balanced Salt Solution (HBSS, Hyclone), incubated in 0.05% trypsin/0.53 mM EDTA (Gibco) for 5 min, and replated in fresh growth medium at a 1:30 dilution. No antibiotics were used and cells were subcultured no more than 100 passages to minimize the artifacts due to cell senescence. Viability of cell populations, as determined by trypan blue exclusion, at the time of experiments always approached 100%. In all the experiments performed in this paper, BHK cells were plated at a density of $5\times10^5$ cells/well in 6-well culture plates, except if stated otherwise, 1 day before infection.

### *Virus preparation and plaque assay*

Recombinant vesicular stomatitis virus that expresses green fluorescence protein at the first position after 3′ leader (VSV-GFP) was generously provided by Sean Whelan (Harvard). The virus was recovered from cDNA clones that have been engineered to express an additional transcriptional unit, purified and amplified in BHK cells, as previously described (Whelan et al., 2000).

Serial 10-fold dilutions of VSV-GFP were made in infection medium consisting of MEM, 2% FBS and 2 mM Glu. Monolayers were infected with 200 µl of virus suspension and incubated for 1 h with gentle rocking every 20 min to keep the monolayers moist and to distribute the virus evenly. Then the inoculum was removed. The monolayers were rinsed with HBSS and overlaid with 2 ml of 0.6% agar (w/v). For the overlay, agar noble (Becton Dickinson) was hydrated with ultrapure water (deionized water, >18.2 mΩcm resistivity, 10% of the desired final volume) and sterilized by autoclaving at 121 °C for 10 min. The sterile agar solution was combined with infection medium at 42 °C to make the overlay mixture. The plates were incubated at 37 °C for approximately 24 h and then fixed with paraformaldehyde (PFA) solution consisting of 4% PFA (w/v) and 5% sucrose (w/v) in 10 mM phosphate buffered saline (PBS, Sigma). After 3 h, the agar overlay was removed and the monolayers were rinsed twice with PBS and stained with 0.1% crystal violet in 20% ethanol for 30 min to visualize plaques. Virus infectivity titers were expressed as plaque forming unit (PFU) per ml.

### *GFP detection and fluorescence-activated cell sorting (FACS)*

BHK cells were infected with 200 µl of VSV-GFP at MOI 0.01. The inoculum was removed after 1 h of adsorption. The cells were then rinsed twice with HBSS and overlaid with 2 ml of infection medium. At indicated times post infection, cells were released using 0.05% trypsin/0.53 mM EDTA, resuspended in infection medium, transferred to 12×75 mm, 5 ml polypropylene round-bottom tubes (Evergreen Scientific) and settled on ice. The cells were filtered right before analysis using cell strainer 40 µm (BD Falcon). Detection and quantification of GFP signal was performed with $\sim3\times10^4$ cells per condition, using a MoFlo cell sorter (DakoCytomation, Fort Collins, CO) at 12 psi with Summit software version 4.13 under biosafety level-3 (BL-3) conditions. The gate for the definition of GFP-positive cells was positioned such that 0.1% of the cells without expressing GFP were positive. Meanwhile, cell viability was measured with propidium iodide (PI, Molecular Probes) staining. Data was acquired based on gated cells, using Flowjo 7.1 software (Tree Star, Inc).

In general, cells were sorted by using the MoFlo cell sorter and then cultured in infection medium at 37 °C. To acquire the yield size distribution, GFP-positive cells were sorted individually into 48-well culture plates with 200 µl of infection medium per well and the supernatants were harvested at 24 h post infection (HPI).

### *One-step virus growth*

Growth medium was removed and 200 µl of virus suspension was applied at MOI 5 on the cell monolayers, ensuring increases in virus titer in the supernatant would reflect amplification from a single round of infection. After 1 h of adsorption at 37 °C with periodic rocking, the inoculum was removed. The cells were then rinsed twice with HBSS (1 ml/rinse) to remove unbound virus and overlaid with 2 ml of infection medium. A sample of 200 µl was taken at 1- or 2-h intervals for 24 h. Two replicates were performed for each time point and all samples were stored at −80 °C until plaque assay.

To measure the one-step growth curve of the sorted cells, groups of 500 cells infected with VSV-GFP at MOI 5 were randomly selected from the live cell population whether they were GFP-positive or not and sorted into 24-well culture plates with 2 ml of infection medium per well. Samples of 200 µl were taken at 1- or 2-h intervals for 24 h. Two replicas were performed for each time point.

### *Virus amplification and characterization*

Viral progeny produced by individual sorted cells were titered by plaque assay. Fifteen viral isolates including seven low yielders (below 500 PFU/cell) and eight high yielders (over 4500 PFU/cell) were amplified at low MOI, as follows. For the first passage, BHK cells were seeded at a density of $2\times10^4$ cells/well in 96-well culture plates 1 day before infection. The monolayers were then overlaid with 100 µl of virus suspension at MOI 0.002±0.001 for low yielders and 0.03±0.01 for high yielders. Supernatants were harvested when cells were all lysed, that is, approximately 40 HPI for low yielders and 30 HPI for high yielders respectively, and titered by plaque assay. For the second passage, BHK cells were seeded at $1.25\times10^6$ cells per T-25 flask 1 day before infection. The monolayers were then overlaid with 5 ml of virus diluted from the first passage at MOI 0.01. Supernatants were harvested at 36 HPI when cells were all lysed and stored at −80 °C as stocks.

### *Plaque-size measurements*

Images of infected cell monolayers were acquired using an HP ScanJet ADF C6270A digital scanner. Plaques were seen as bright dots against dark background. Scion Image Beta 4.03 was used to measure the plaque sizes. About 80 plaques were measured for each virus isolate.

### *Effects of cell size on virus yield*

BHK cells infected with VSV-GFP at MOI 5 were divided into three groups based on their forward scatter (FSC) intensity and pulse width from live cell population at 3 HPI. 90% of the total cells were gated as individual cells based on their forward scatter (FSC) and side scatter (SSC), divided into three groups based on their FSC intensity and pulse width. The high-, medium- and low-FSC populations accounted for 25, 50 and 25% of the gated cells, respectively. The mean value of FSC intensity was calculated for each group. Cells from each group were sorted into a 24-well plate at approximately $2\times10^4$ cells per well with 1 ml of infection medium. After 10 min, when the cells had settled to the surface of the culture well but not yet flattened out, images were taken at 10× magnification by a Nikon Eclipse TE300 inverted epifluorescent microscope equipped with a monochrome SensSys 4.0 cooled CCD camera driven by MetaMorph 4.0 software (Universal Imaging). The diameters of approximately 100 cells were manually measured from the phase-contrast images and averaged for each group.

To measure the virus yield, cells from each group were sorted into 24-well plates at 500 cells per well with 2 ml of infection medium. Supernatants were sampled at 24 HPI and stored at −80 °C until virus yields were determined by plaque assay. Four replicas were performed for each group.

*Correlation of virus yield with cell cycle*

*Synchronization of cell population*

BHK cells were seeded at $2\times10^5$ cells/well in six-well culture plates and grown in medium with 10% serum (standard growth medium) at 37 °C. After 24 h, cells were rinsed once with HBSS and grown in medium with 2% serum. After 12 h, cells were rinsed once with HBSS and cultured in serum-free medium. After a 12 h serum starvation period, cells were treated with standard growth medium containing 5 μg/ml aphidicolin (Sigma; freshly prepared at 5 mg/ml in DMSO) for 12 h, to block the cells at $G_1$/S boundary. The cells were released from the aphidicolin block by washing with HBSS three times (1 ml per wash) prior to incubation in standard growth medium.

*Cell cycle analysis*

Cells were synchronized as described above. Every 2 h in a 12 h period after drug removal, cells from one plate were dislodged by trypsinization and then either counted by trypan blue exclusion or resuspended in 70% ethanol. The fixed samples were kept at −20 °C until ready for PI staining. PI staining solution was composed of 1 mg/ml RNase A, 33 μg/ml PI, and 0.2% (v/v) Triton X 100, in PBS. The stained samples were analyzed by a FACSCalibur benchtop analyzer equipped with 488 nM and 633 nM lasers. The DNA histograms show the number of cells per channel in the ordinate and the relative fluorescence intensity which varies in proportion with the DNA content in the abscissa. The contribution of each cell phase to the observed signal was estimated using MODFIT LT (Verity Software House, Topsham, ME). Beforehand, the DNA content of a non-synchronized cell population was analyzed to locate the $G_0G_1$ channel assuming that the majority of the cells were in this phase. The position of that $G_2$M channel was then determined given that the amount of DNA content of the cells in this phase was twice of that in G0G1.

*Measurement of viral productivity in different phases of the cell cycle*

Cells were synchronized as described above. Every 2 h during a 12 h period after drug removal cells from one plate were infected with VSV-GFP at MOI 5. Supernatants were sampled after 24 HPI and measured by plaque assay. The virus yield ($y$) at each time point was fit with a superposition model that assumed the total yield reflected the sum of yields of virus from cells in each of the four phases:

$$y = ax_1 + bx_2 + cx_3 + dx_4$$

where $x_1$, $x_2$, $x_3$ and $x_4$ were the fraction of cells in phases $G_2$M, late S, early S and $G_0G_1$, respectively, determined by our cell cycle analysis. The corresponding yields ($a$, $b$, $c$ and $d$) were estimated by multiple regression of yield data from the seven data points.

*Statistical analysis*

Data were expressed as mean ± standard deviation. The difference between a number and a group was analyzed by Student's $t$ distribution. $P<0.05$ was considered statistically significant.

## Acknowledgments

We thank James F. Crow for comments on the manuscript, Eva Rakasz for assistance with cell sorting, and Kathy Schell for advice on cell-cycle analysis. Herlina Moeljadi contributed technical assistance in the initial stages of this work. Sean Whelan provided the recombinant GFP strain of VSV. The BL-3 cell sorter facility is supported by the Wisconsin National Primate Research Center (National Institutes of Health 5P51-RR000167-46), and the University of Wisconsin Comprehensive Cancer Center flow cytometry facility is supported by an NIH core grant (CA014520-32). This work was supported by an NIH Phased Innovation Award (AI071197) and an NSF Focused Research Group Award (DMS-0553687).

## Appendix A. Supplementary data

Supplementary data associated with this article can be found, in the online version, at doi:10.1016/j.virol.2008.10.031.

## References

Aaskov, J., Buzacott, K., Thu, H.M., Lowry, K., Holmes, E.C., 2006. Long-term transmission of defective RNA viruses in humans and *Aedes* mosquitoes. Science 311 (5758), 236–238.

Arkin, A., Ross, J., McAdams, H.H., 1998. Stochastic kinetic analysis of developmental pathway bifurcation in phage lambda-infected *Escherichia coli* cells. Genetics 149 (4), 1633–1648.

Blondel, D., Harmison, G.G., Schubert, M., 1990. Role of matrix protein in cytopathogenesis of vesicular stomatitis virus. J. Virol. 64 (4), 1716–1725.

Butel, J.S., 2000. Viral carcinogenesis: revelation of molecular mechanisms and etiology of human disease. Carcinogenesis 21 (3), 405–426.

Carrillo, C., Lu, Z., Borca, M.V., Vagnozzi, A., Kutish, G.F., Rock, D.L., 2007. Genetic and phenotypic variation of foot-and-mouth disease virus during serial passages in a natural host. J. Virol. 81 (20), 11341–11351.

Chao, L., 1990. Fitness of RNA virus decreased by Muller's ratchet. Nature 348 (6300), 454–455.

Clarke, D., Duarte, E., Moya, A., Elena, S., Domingo, E., Holland, J., 1993. Genetic bottlenecks and population passages cause profound fitness differences in RNA viruses. J. Virol. 67 (1), 222–228.

Cuevas, J.M., Moya, A., Sanjuan, R., 2005. Following the very initial growth of biological RNA viral clones. J. Gen. Virol. 86 (Pt 2), 435–443.

Davy, C., Doorbar, J., 2007. G2/M cell cycle arrest in the life cycle of viruses. Virology.

Delbrück, M., 1945. The burst size distribution in the growth of bacterial viruses (bacteriophages). J. Bacteriol. 50, 131–135.

Demma, L.J., Logsdon Jr., J.M., Vanderford, T.H., Feinberg, M.B., Staprans, S.I., 2005. SIVsm quasispecies adaptation to a new simian host. PLoS Pathog. 1 (1), e3.

Domingo, E., 2003. Quasispecies and the development of new antiviral strategies. Prog. Drug Res. 60, 133–158.

Domingo, E., Martinez-Salas, E., Sobrino, F., Torre, J.C.d.l., Portela, A., Ortin, J., Lopez-Galindez, C., Perez-Brena, P., Villanueva, N., Najera, R., VandePol, S., Steinhauer, D., DePolo, N., Holland, J., 1985. The quasispecies (extremely heterogeneous) nature of viral RNA genome populations: biological relevance—a review. Gene 40, 1–8.

Dove, B., Brooks, G., Bicknell, K., Wurm, T., Hiscox, J.A., 2006. Cell cycle perturbations induced by infection with the coronavirus infectious bronchitis virus and their effect on virus replication. J. Virol. 80 (8), 4147–4156.

Drake, J.W., Holland, J.J., 1999. Mutation rates among RNA viruses. Proc. Natl. Acad. Sci. U. S. A. 96 (24), 13910–13913.

Duarte, E., Clarke, D., Moya, A., Domingo, E., and Holland, J., 1992. Rapid fitness losses in mammalian RNA virus clones due to Muller's ratchet. National Academy of Sciences, Washington, D.C, Proceedings 89(13), 6015–6019.

Duarte, E.A., Clarke, D.K., Moya, A., Elena, S.F., Domingo, E., Holland, J., 1993. Many-trillionfold amplification of single RNA virus particles fails to overcome the Muller's ratchet effect. J. Virol. 67 (6), 3620–3623.

Duffy, S., Turner, P.E., Burch, C.L., 2006. Pleiotropic costs of niche expansion in the RNA bacteriophage phi 6. Genetics 172 (2), 751–757.

Elena, S.F., Moya, A., 1999. Rate of deleterious mutation and the distribution of its effects on fitness in vesicular stomatitis virus. J. Evol. Biol. 12 (6), 1078–1088.

Elena, S.F., Gonzalez-Candelas, F., Novella, I.S., Duarte, E.A., Clarke, D.K., Domingo, E., Holland, J.J., Moya, A., 1996. Evolution of fitness in experimental populations of vesicular stomatitis virus. Genetics 142 (3), 673–679.

Farci, P., Shimoda, A., Coiana, A., Diaz, G., Peddis, G., Melpolder, J.C., Strazzera, A., Chien, D.Y., Munoz, S.J., Balestrieri, A., Purcell, R.H., Alter, H.J., 2000. The outcome of acute hepatitis C predicted by the evolution of the viral quasispecies. Science 288 (5464), 339–344.

Foisy, S., Bibor-Hardy, V., 1988. Synthesis of nuclear lamins in BHK-21 cells synchronized with aphidicolin. Biochem. Biophys. Res. Commun. 156 (1), 205–210.

Gohara, D.W., Arnold, J.J., Cameron, C.E., 2004. Poliovirus RNA-dependent RNA polymerase (3Dpol): kinetic, thermodynamic, and structural analysis of ribonucleotide selection. Biochemistry 43 (18), 5149–5158.

Goodenow, M., Huet, T., Saurin, W., Kwok, S., Sninsky, J., Wain-Hobson, S., 1989. HIV-1 isolates are rapidly evolving quasispecies: evidence for viral mixtures and preferred nucleotide substitutions. J. Acquir. Immune Defic. Syndr. 2 (4), 344–352.

Holland, J., 1993. Replication error, quasispecies populations, and extreme evolution rates of RNA viruses. In: Morse, S. (Ed.), Emerging Viruses. Oxford Univ. Press, New York, pp. 203–218.

Holland, J.J., Spindler, K., Horodyski, F., Grabau, E., Nichol, S., VandePol, S., 1982. Rapid evolution of RNA genomes. Science 215, 1577–1585.

Larder, B.A., Kemp, S.D., 1989. Multiple mutations in HIV-1 reverse transcriptase confer high-level resistance to zidovudine (AZT). Science 246 (4934), 1155–1158.
Marcus, P.I., Rodriguez, L.L., Sekellick, M.J., 1998. Interferon induction as a quasispecies marker of vesicular stomatitis virus populations. J. Virol. 72 (1), 542–549.
Miralles, R., Gerrish, P.J., Moya, A., Elena, S.F., 1999. Clonal interference and the evolution of RNA viruses. Science 285 (5434), 1745–1747.
Nichol, S.T., Rowe, J.E., Fitch, W.M., 1989. Glycoprotein evolution of vesicular stomatitis virus New Jersey. Virology 168 (2), 281–291.
Novella, I.S., Ebendick-Corpus, B.E., 2004. Molecular basis of fitness loss and fitness recovery in vesicular stomatitis virus. J. Mol. Biol. 342 (5), 1423–1430.
Novella, I.S., Hershey, C.L., Escarmis, C., Domingo, E., Holland, J.J., 1999. Lack of evolutionary stasis during alternating replication of an arbovirus in insect and mammalian cells. J. Mol. Biol. 287 (3), 459–465.
Novella, I.S., Gilbertson, D.L., Borrego, B., Domingo, E., Holland, J.J., 2005. Adaptability costs in immune escape variants of vesicular stomatitis virus. Virus Res. 107 (1), 27–34.
Novella, I.S., Ebendick-Corpus, B.E., Zarate, S., Miller, E.L., 2007. Emergence of mammalian cell-adapted vesicular stomatitis virus from persistent infections of insect vector cells. J. Virol. 81 (12), 6664–6668.
Parrish, C.R., Kawaoka, Y., 2005. The origins of new pandemic viruses: the acquisition of new host ranges by canine parvovirus and influenza A viruses. Annu. Rev. Microbiol. 59, 553–586.
Pedrali-Noy, G., Spadari, S., Miller-Faures, A., Miller, A.O., Kruppa, J., Koch, G., 1980. Synchronization of HeLa cell cultures by inhibition of DNA polymerase alpha with aphidicolin. Nucleic Acids Res. 8 (2), 377–387.
Pfeiffer, J.K., Kirkegaard, K., 2006. Bottleneck-mediated quasispecies restriction during spread of an RNA virus from inoculation site to brain. Proc. Natl. Acad. Sci. U. S. A. 103 (14), 5520–5525.
Poon, A.F., Chao, L., 2006. Functional origins of fitness effect-sizes of compensatory mutations in the DNA bacteriophage phiX174. Evolution Int. J. Org. Evolution 60 (10), 2032–2043.
Quer, J., Hershey, C.L., Domingo, E., Holland, J.J., Novella, I.S., 2001. Contingent neutrality in competing viral populations. J. Virol. 75 (16), 7315–7320.
Sanjuan, R., Cuevas, J.M., Furio, V., Holmes, E.C., Moya, A., 2007. Selection for robustness in mutagenized RNA viruses. PLoS Genet. 3 (6), e93.
Sharpless, T.K., Melamed, M.R., 1976. Estimation of cell size from pulse shape in flow cytofluorometry. J. Histochem. Cytochem. 24 (1), 257–264.
Srivastava, R., You, L., Summers, J., Yin, J., 2002. Stochastic versus deterministic modeling of intracellular viral kinetics. J. Theor. Biol. 218 (3), 309–321.
Steinhauer, D., de la Torre, J., Meier, E., Holland, J., 1989. Extreme heterogeneity in populations of vesicular stomatitis virus. J. Virol. 63 (5), 2072–2080.
Steinhauer, D.A., Domingo, E., Holland, J.J., 1992. Lack of evidence for proofreading mechanisms associated with an RNA virus polymerase. Gene 122 (2), 281–288.
Thomas, D., Newcomb, W.W., Brown, J.C., Wall, J.S., Hainfeld, J.F., Trus, B.L., Steven, A.C., 1985. Mass and molecular composition of vesicular stomatitis virus: a scanning transmission electron microscopy analysis. J. Virol. 54 (2), 598–607.
Tyrer, H.W., Kunkel-Berkley, C., 1984. Multiformat electronic cell sorting system; I. Theoretical considerations. Rev. Sci. Instrum. 55 (7), 1044–1050.
Vignuzzi, M., Stone, J.K., Arnold, J.J., Cameron, C.E., Andino, R., 2006. Quasispecies diversity determines pathogenesis through cooperative interactions in a viral population. Nature 439 (7074), 344–348.
Weinberger, L.S., Burnett, J.C., Toettcher, J.E., Arkin, A.P., Schaffer, D.V., 2005. Stochastic gene expression in a lentiviral positive-feedback loop: HIV-1 Tat fluctuations drive phenotypic diversity. Cell 122 (2), 169–182.
Whelan, S.P., Barr, J.N., Wertz, G.W., 2000. Identification of a minimal size requirement for termination of vesicular stomatitis virus mRNA: implications for the mechanism of transcription. J. Virol. 74 (18), 8268–8276.
Yen, H.L., Herlocher, L.M., Hoffmann, E., Matrosovich, M.N., Monto, A.S., Webster, R.G., Govorkova, E.A., 2005. Neuraminidase inhibitor-resistant influenza viruses may differ substantially in fitness and transmissibility. Antimicrob. Agents Chemother. 49 (10), 4075–4084.